The two-domain model of solute transport in binary alloy

Mirosław Seredyński[1,*], and *Jerzy* Banaszek[1]

[1]Institute of Heat Engineering, Warsaw University of Technology, 21/25 Nowowiejska Str., 00-665 Warsaw, Poland

Abstract. A mixed model for micro-macroscopic computer simulation of binary alloy solidification is proposed. It involves a two-domain approach to solute conservation equations in the liquid and solid phases, whereas transport of momentum and energy in the two-phase region is modelled using the phase mixture theory. To distinguish regions of columnar and equiaxed crystal structures evolving in a cast during solidification, the special front tracking technique on non-structural triangular grids is included in the model. In this two-domain approach, solute conservation equations are averaged across solid and liquid phases, and the solute transport at the phase interface is included. Additionally, the microstructure evolution is modelled to capture the development of various complex grain structures and more accurately describe the solute transport between the phases. The accuracy of the proposed model is first verified by a grid refinement analysis, and then the model is used to predict the solute concentration and macro-segregation in the example problem of Pb-48%wt Sn alloy solidification in a 2D mould. The results obtained are next compared with the relevant ones predicted by the fully single-domain model, earlier developed by authors. Thus, the role of finite diffusion in liquid and solid phases is identified and discussed.

1 Introduction

Solidification of binary alloys is a complex process, which involves multiscale transport phenomena and formation of a complex tiny tree-like microstructure of the solid phase. Its morphology can be columnar or equiaxed. The former one develops close to cooled walls and these grains grow towards the mould interior. In front of them, in the undercooled liquid, globular grains can appear and they evolve into equiaxed crystals. Columnar dendrites are stationary, whereas equiaxed grains can be freely transported with the ambient, melt. Within these two macroscopic regions of different grain structures distinct flow conditions and transport properties occur, so they should be treated separately and individually - as a porous medium and slurry of solid grains, respectively. Hence, the important part of micro-macroscopic modelling of alloy solidification is the identification of zones of different grain morphology by tracing of a moving hypothetical interface separating these zones. In their advanced multi-phase model Wang and Beckermann [1] used a simple one-dimensional approach of the single point tracking of the liquidus isotherm, justified only for diffusive heat and mass transport. Browne and Hunt [2], in their model of diffusion driven binary alloy solidification, introduced tracing of a line separating the columnar dendrite region from the undercooled zone on a regular control volume grid. The line, consisting of connected linear segments, being a locus of the envelope of columnar dendrite tips, represented by mass-less markers moving across the domain according to prescribed kinetics. This approach was further extended to the cases involving thermal natural convection (Banaszek and Browne [3]), thermo-solutal natural convection (Seredyński and Banaszek [4,5]) and non-structural triangular control volume grids (Seredyński and Banaszek [6]). Their model took into account micro- and macroscopic transport of solute, equilibrium growth of solid grains in the undercooled liquid, blocking of growth of columnar dendrites with equiaxed grains, and it replaced the commonly used coherency point model (e.g. Ilegbusi and Mat [7]) by more exact distinguishing the zones of different dendrite structures [5].

However, since the model is based on the mixture theory, where local thermal and solutal equilibrium is assumed, many microscale phenomena are beyond its scope, like nucleation, globular/equiaxed growth, solute transport rate at the phase boundary related to evolving grain shape, etc.

Several recently developed models, which are based on the volume averaging and the multi-domain approach, enable modelling of these nonequilibrium processes. The basic equations have been developed by Ganesan and Poirier [8] and Ni and Beckermann [9]. They have been further generalized for multi-phase systems (for example [10]), and implemented in the commercial software (for example [11]).

The paper presents an updated model for micro-macroscopic computer simulation of binary alloy solidification, which preserves the computational efficiency of the single domain mixture model. It is based on a two-domain approach to solute conservation equations in the liquid and solid phases, whereas

* Corresponding author: Miroslaw.Seredynski@pw.edu.pl

transport of momentum and energy in the two-phase region (mushy zone) is modelled on the basis of the mixture theory. To distinguish regions of different crystal structures evolving in a mould during solidification, the front tracking technique on non-structural triangular grids, earlier developed by the authors ([4-6]), is included in the model. Its accuracy is verified by the grid independency study, and its predictions of solute concentration fields and macro-segregation with potential channeling are compared with the relevant results obtained from the fully equilibrium mixture model, for the selected example problem of Pb-48%wt Sn alloy solidification in a 2D mould.

2 Mathematical model

Mathematical model takes into account mass, momentum, energy and solute transport in the two-phase medium during solidification. The procedure of front tracking is also used to separate regions in the two-phase domain, where various dendrite morphologies prevail. The idea and details of its implementation are discussed in the next section. The mathematical model used here is refers to the previous ones developed by authors.

2.1 Transport equations

The momentum and energy transfer are assumed to be equilibrium processes. It can be justified with relatively low velocities of the molten alloy and high Lewis number, typical for metal alloys, so the averaged across both phases transport equations of mass, momentum and energy can be expressed in the form (e.g. [5])

$$\nabla \cdot \mathbf{V} = 0 \tag{1}$$

$$\begin{aligned}\frac{\partial(\rho\mathbf{V})}{\partial t} + \nabla\cdot(\rho\mathbf{V}\mathbf{V}) &= \nabla\cdot(\mu_l\nabla\mathbf{V}) \\ -\nabla\cdot(\mu_l f_s\nabla\mathbf{V}_s) &+ \nabla\cdot(\mu_s f_s\nabla\mathbf{V}_s) \\ -\nabla\cdot\left[\rho\frac{f_s}{f_l}(\mathbf{V}-\mathbf{V}_s)(\mathbf{V}-\mathbf{V}_s)\right] & \\ +\rho\mathbf{B} + \left(1-g_s\tilde{V}\right)\nabla p - \mu_l g_l K^{-1}\mathbf{V}\tilde{V} &\end{aligned} \tag{2}$$

$$\begin{aligned}\frac{\partial(\rho cT)}{\partial t} + \nabla\cdot(\rho c\mathbf{V}T) &= \nabla\cdot(k\nabla T) \\ +\rho L\frac{\partial f_s}{\partial t} - \rho L\nabla\cdot(f_l\mathbf{V}_l) &\end{aligned} \tag{3}$$

The mass balance equation of the solid phase is based on the volume averaging procedure of the microscale mass balance equation and reflects findings presented in [9] and [10]

$$\frac{\partial g_s}{\partial t} + \nabla\cdot(g_s\mathbf{V}_s) = \frac{\Gamma_s}{\rho} \tag{4}$$

where $\mathbf{V}_s$ is the local intrinsic volume average velocity of solid phase and Γ_s is the mass flux of solid phase per unit volume at the phase interface due to phase change. The term related to the effect of nucleation is neglected here.
The solute transport equations are established in solid and liquid phases separately. The equation are based on the volume averaging procedure performed over solid and liquid phases (e.g. [9,10])

$$\frac{\partial(g_s C_s)}{\partial t} + \nabla\cdot(g_s\mathbf{V}_s C_s) = \frac{1}{\rho}\left(J_s^d + J_s^\Gamma\right) \tag{5}$$

$$\frac{\partial(g_l C_l)}{\partial t} + \nabla\cdot(g_l\mathbf{V}_l C_l) = \frac{1}{\rho}\left(J_l^d + J_l^\Gamma\right) \tag{6}$$

where J_s^d and J_l^d are the interfacial fluxes of solute per unit volume due to diffusion on the solid and liquid sides of the phase interface, respectively. Similarly, J_s^Γ and J_l^Γ are the interfacial fluxes of solute per unit volume due to phase change on both sides of the phase interface. In eq. (5) and (6) terms related to the solid grains nucleation are neglected. Presented above equations need additional relations, closure data, which are discussed in following sections.

2.2 Modelling of fluid flow

The single momentum balance equation (2) describes the fluid flow in the whole domain. In the region where two-phases coexist two zones are identified, with columnar dendrites and equiaxed grains. In those zones two different flow regimes are distinguished. In the columnar dendrites zone the solid phase is stationary and the character of flow is typical for porous medium. In this domain the permeability, K, is defined, and described with the formula

$$K = \frac{\lambda_2^2(1-g_s)^3}{180 g_s^2} \tag{7}$$

Average velocity of the solid phase in this region is equal to zero. In the second part of the two-phase domain, solid grains are immersed in the undercooled liquid, and the model of slurry flow is utilized. The mechanical equilibrium between phases is assumed, so averaged phase velocities are taken to be equal, $\mathbf{V}_s$=$\mathbf{V}_l$. It is justified with relatively small size of the domain and low velocities of the two-phase mixture.
In the liquid and solid phases buoyancy forces appear due to variation of liquid density with temperature and composition. The simple Boussinesq model is used

$$\begin{aligned}\rho\mathbf{B} = g_l\rho_{l,ref}\mathbf{g}&\begin{bmatrix}\beta_{T,l}(T-T_{ref}) \\ +\beta_{C,l}(C_l - C_{l,ref})\end{bmatrix} + \\ +\left(1-\tilde{V}\right)g_s\rho_{s,ref}\mathbf{g}&\begin{bmatrix}\beta_{T,s}(T-T_{ref}) \\ +\beta_{C,s}(C_s - C_{s,ref})\end{bmatrix}\end{aligned} \tag{8}$$

2.3 Modelling of mass transfer at the phase boundary

Two mechanisms of solute transport at the phase boundary are accounted for, namely related to solutal diffusion across the interface and the phase boundary motion due to phase change. Additionally, the simple nucleation mechanism is considered to capture the onset of solidification. All mentioned processes are tightly related to microscopic evolution of grains.

2.3.1 Nucleation

The simple nucleation model is applied. Solidification starts when local temperature drops below the onset of solidification temperature. It is defined as the difference in local liquidus temperature and prescribed undercooling, ΔT_{liq}. In this study the value of ΔT_{liq} was equal to 0.1 K.

2.3.2 Interphase solute diffusion

The simple diffusive transport is adopted based on the model presented in [9]. The diffusion flux on the side of the phase k (solid or liquid) is related to the difference between the concentration at the phase interface and the average concentration in phase k

$$J_k^d = \frac{S_v D_k}{\delta_k}\left(C_k^* - C_k\right) \tag{9}$$

where S_v is the interfacial area density. For globular grains it can be expressed as

$$S_{v,e} = \begin{cases} \pi d_g^2 N & g_s \le g_{s,c} \\ \pi d_g^2 N \left(\frac{g_s}{g_{s,c}}\right)^{\frac{1}{3}} \left(\frac{1-g_s}{1-g_{s,c}}\right)^{\frac{1-g_{s,c}}{g_{s,c}}} & g_s > g_{s,c} \end{cases} \tag{10}$$

where $g_{s,c}$ is the volumetric fraction of solid phase, at which packing of grains occurs. For columnar dendrites simple formula is adopted [9]

$$S_{v,c} = \frac{2}{\lambda_2} \tag{11}$$

Diffusion lengths close to globular/equiaxed grains were calculated with the formulae taken from [9]

$$\delta_{l,e} = \frac{d_g}{2}\min\left[1, \left(\frac{1}{1-g_s^{1/3}} + \frac{Sc^{1/3}\,\mathrm{Re}^a}{3g_l}\right)^{-1}\right] \tag{12}$$

$$\delta_{s,e} = \frac{d_g}{10}$$

where Schmidt and Reynolds numbers and parameter a were determined with the formulae

$$\mathrm{Re} = \frac{\rho g_l d_g}{\mu_l}\left|\mathbf{V}_l - \mathbf{V}_s\right|; \quad Sc = \frac{\mu_l}{D_l}; \qquad a = \frac{2\,\mathrm{Re}^{0.28} + 4.65}{3\left(\mathrm{Re}^{0.28} + 4.65\right)} \tag{13}$$

Diffusion lengths in the columnar zone are determined with the formula [9]

$$\delta_{l,c} = \delta_{s,c} = \frac{g_s \lambda_2}{6} \tag{14}$$

2.3.3 Solute transport due to phase change

The solute transfer at the phase interface is determined by

$$J_k^\Gamma = C_k^* \Gamma_k \tag{15}$$

where phase change rate in the solid and liquid phases accomplishes the relation, $\Gamma_s = -\Gamma_l$. It is determined with the mass balance at the phase boundary,

$$J_s^d + J_s^\Gamma + J_l^d + J_l^\Gamma = 0 \tag{16}$$

If the equilibrium solute composition at the phase interface is assumed, namely $C_s^* = k_p C_l^*$, and the thermal equilibrium at the interface, $T = T_M + m_l C_l^*$, the solute balance equation at the interface becomes

$$\left(k_p - 1\right) C_l^* \Gamma_s = \frac{S_v D_l}{\delta_l}\left(C_l - C_l^*\right) + \frac{S_v D_s}{\delta_s}\left(C_s - k_p C_l^*\right) \tag{17}$$

3 Front tracking procedure

Due to existence of two regions where various dendrite morphologies prevail and where different models of fluid flow should be applied, the procedure of identification of these regions is utilized. It is realized with the procedure of tracking the envelope of columnar dendrite tips, which separates both subdomains of the two-phase region. The front is defined as the sequence of linear segments connected with mass-less markers. Markers move according to prescribed dendrite tip kinetics, which is a relation between solutal undercooling and dendrite tip growth rate. For the alloy Pb-48wt%Sn the relation reads [5]:
$V_t = 1.689 \cdot 10^{-7} \Delta T^2 + 1.217 \cdot 10^{-7} \Delta T^3$ where
$\Delta T = T_m + m_l C - T$. On the basis of the actual position of the front the switching function, $\tilde{V}$, is determined in control volumes crossed by the front. This function determined for each control volume expresses which part of the c.v. is behind the front. It is equal to 0 in these cells which are entirely immersed in the undercooled liquid and 1 in the cells placed entirely in columnar

dendrites zone. The idea of the front tracking procedure and its relation to the momentum balance equation have been presented in [5] for the mapped c.v. meshes and in [6] for the non-orthogonal, triangular c.v. meshes. In the proposed model the switching function is also used to identify regions where different models of growth of solid phase are imposed.

4 Problem statement

The problem considered here is solidification of binary alloy, Pb-48%wt Sn in a rectangular cavity of length 0.1 m and height 0.06 m, cooled from a side. The Newton-Robine boundary condition for the energy equation is imposed on the left wall; the heat transfer coefficient and the ambient fluid temperature are equal to 400W/(m^{2}K) and 25°C, respectively. All other walls are perfectly insulated and impermeable Initial solute concentration is equal to 48 wt % Sn, initial temperature is 216°C and initial velocity is zero. Material properties used in this case are available elsewhere (e.g. [4-6]). The domain was discretized with uniform, triangular, nonorthogonal c.v. grid, which diameter was set equal to 1 mm, 0.8 mm and 0.5 mm.

Balance equations were integrated on collocated, non-orthogonal, triangular control volume mesh. The transient terms were integrated with implicit Euler scheme. The formula for diffusive fluxes across control volume faces took into account the skewness term [11] resulting from the non-orthogonality of the mesh. To avoid artificial pressure oscillations, the Rhie and Chow [12] scheme was used to evaluate the interfacial convective fluxes.

5 Results and discussion

5.1 Grid sensitivity analysis

Analysis of the role of mesh density was carried out first. Simulations were performed for three uniform and triangular c.v. meshes. Their densities were described with diameter of c.v's, equal to 1.0 mm, 0.8 mm and 0.5 mm. For each case the same time step, equal to 0.01s was used.

In figure 1 contour plots of average solute fraction after 200s of the process are compared. Position of the front is denoted with a black continuous line. Predicted concentrations match well, and positions of the fronts are similar. Tendency to formation of A-segregates is not observed here, but a slightly more enriched in solute region close to the fully solidified alloy is predicted with simulation performed on the finest mesh. Slight differences can be observed in the fully solidified region, close to cooled wall. Only for results predicted using the finest grid, the mesh dependent artefacts in the solute fraction distribution are not observed.

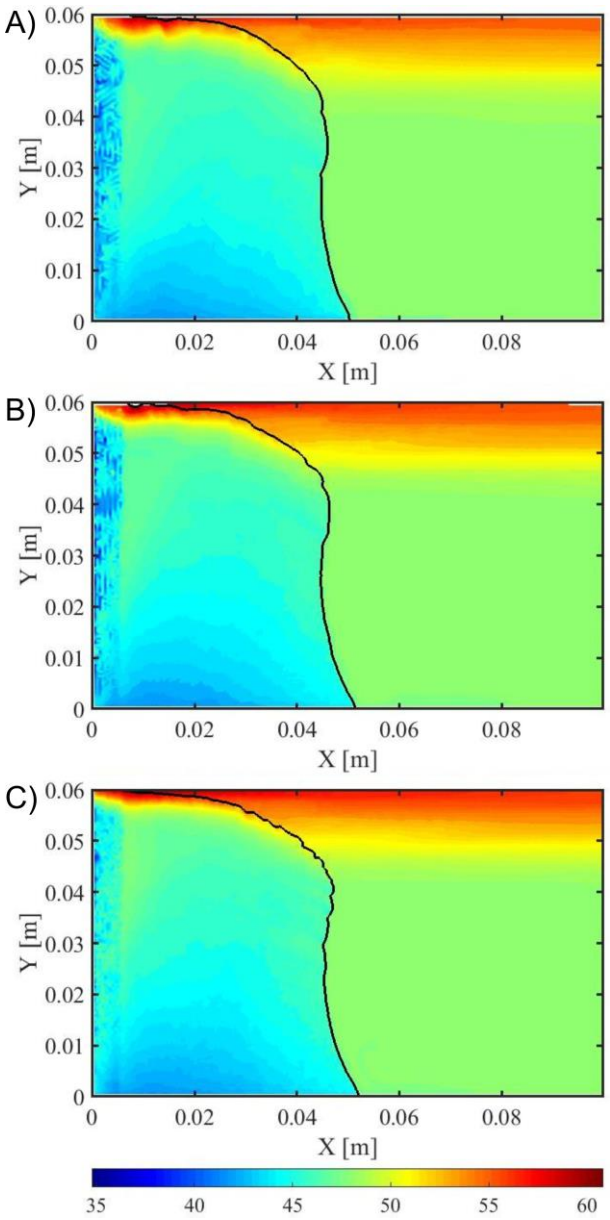

Fig. 1. Contour plots of average solute concentration after 200s of the process predicted with simulations carried out on mesh densities 1.0 mm (A), 0.8 mm (B) and 0.5 mm (C).

5.2 Comparison of the fully equilibrium and proposed models

The proposed, two-domain (T-D) model accounting for the finite solute diffusion in the liquid and solute phases is compared with the fully equilibrium, single-domain (S-D) model. In the latter the Scheil model of microdiffusion is utilized, which is based on the assumption that the mass diffusion in the solid phase is neglected and liquid phase is well mixed. Details of the single-domain computational model of alloy solidification are available elsewhere, for example in [4-6].

Comparison of solid fractions predicted with fully equilibrium (S-D) model and the proposed two-domain (T-D) model are shown in Fig. 2. In spite of various assumptions applied in these models, related to micro-

scale solute transport at the phase boundary, their comparison can supply some insight into underlying processes. Distributions of solute fraction predicted for two time instants, namely 100s and 200s of the process, reveal considerable differences between models in the initial stage, which subsequently diminish in the later stage. The S-D model predicts numerous segregate channels in the initial stage of solidification (Fig. 2A). In the later stage of the process they are partially overgrown by solidifying material (Fig. 2C). The second model (T-D) predicts no segregation channels, but only zone of reduced solid fraction in the mid-height of the domain close to cooled wall (Fig. 2B) which subsequently disappears (Fig. 2D). For each case position of the front close to the upper wall is shifted towards the cooled wall. It is due to developed at the top of the domain zone of enriched in solute liquid alloy, which is predicted with both models (Fig. 1). In the bottom part, growth of the front is retarded due to vigorous convection in the bulk liquid. This effect is more pronounced for results predicted with S-D model, but it diminishes in the later stage (Fig. 2C and D).

Comparison of solute concentrations averaged across both phases predicted with S-D and T-D models (Fig. 3) reveals similar phenomena related to macrosegregation evolution. The vertical segregation is observed in the bulk liquid and the well mixed zone in the bottom part. Some similarities can be found behind the front, in the columnar dendrites zone. In the bottom of this region, a negative segregation develops. The proposed model predicts more intensive segregation in this zone. The crucial difference mentioned earlier is in the prediction of the developing segregation channels by the S-D model, what is not the case in the T-D model. The reason can be related to the physical model of the process. In the fully equilibrium model (S-D model), solidification starts at the local liquidus temperature and next the equilibrium growth of solid grains occurs. So, the solid fraction is tightly related to solute concentration and temperature. That case describes the fastest possible growth of the solid phase in the undercooled liquid. Process of grain growth is also related to the release of solute to the bulk liquid, which is a source of the solutal convection. Stream functions predicted with both models, presented in Fig. 5 for the time of 100s, indicate that solutal convection is more vigorous in the case of the S-D model than the one predicted with the T-D. In that situation, the flow induced in the columnar dendrites zone is more intensive and can promote formation of segregation channels. This issue requires further and more detailed investigation.

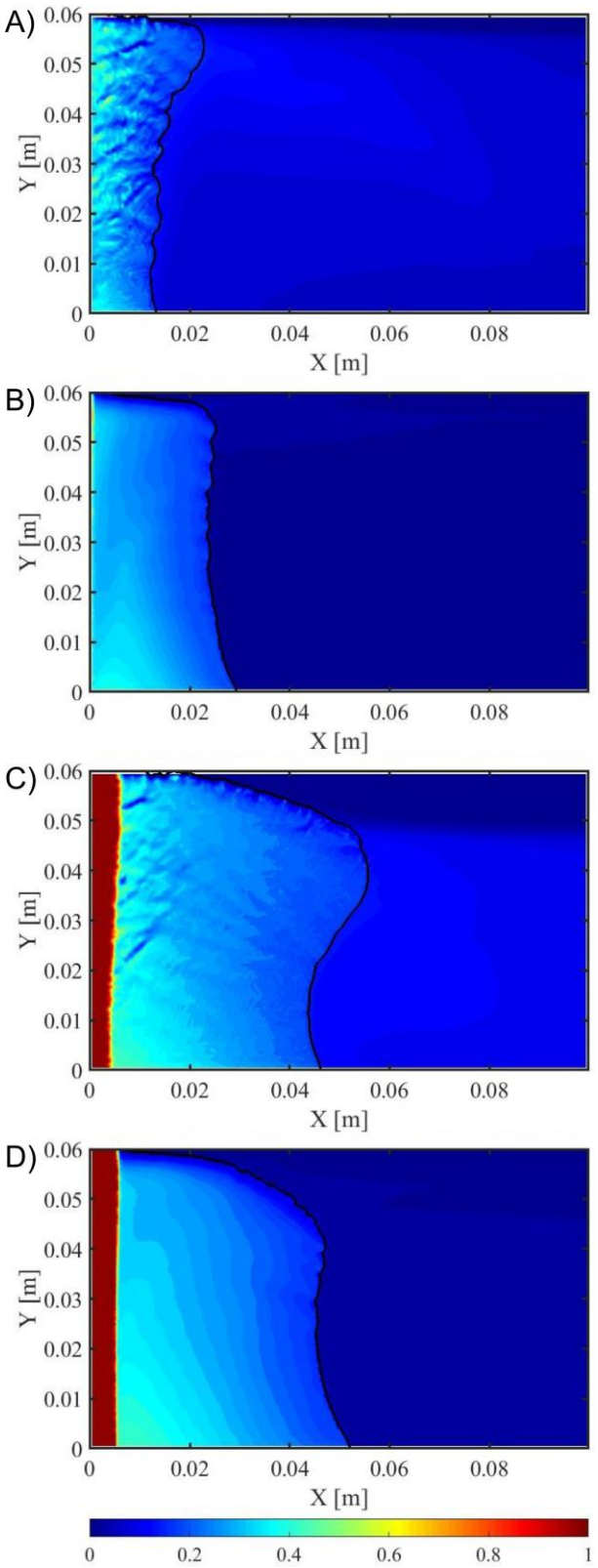

Fig. 2. Contour plots of solid fraction after 100s (A and B) and 200s (C and D) of the process predicted with the S-D model (A and C) and the T-D model (B and D).

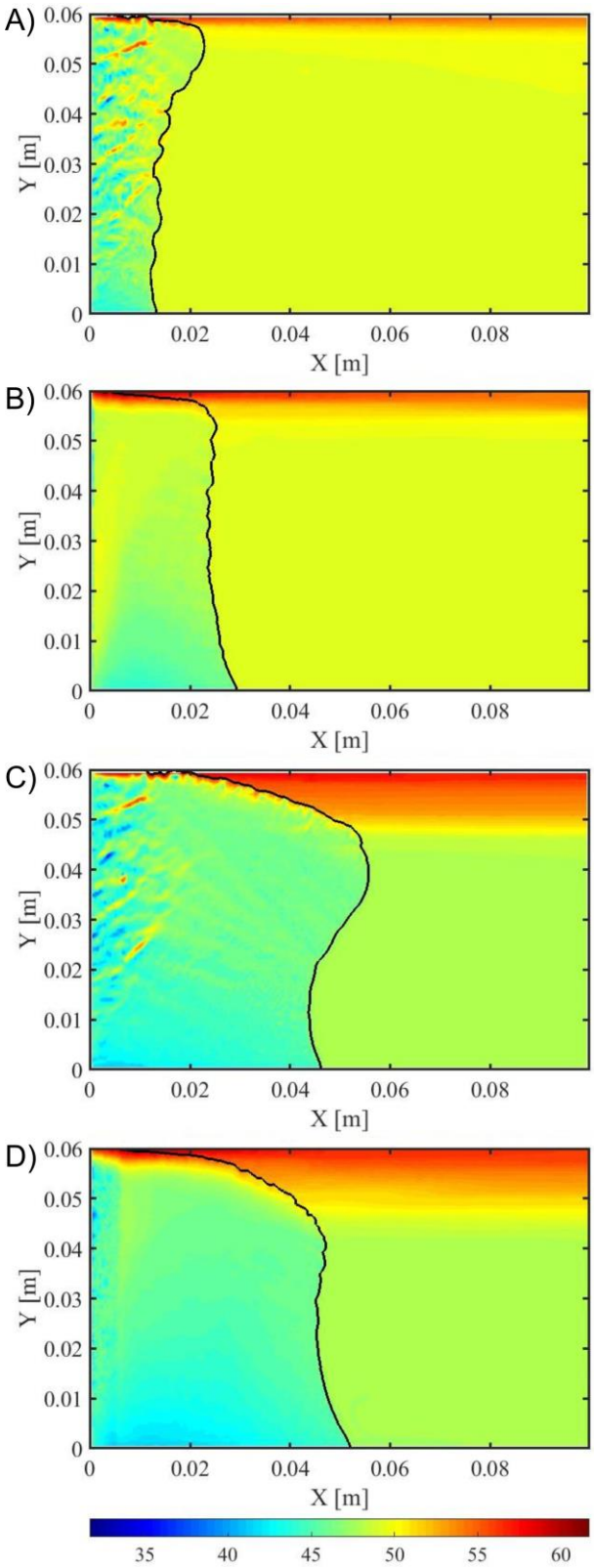

Fig. 3. Contour plots of average solute fraction after 100s (A and B) and 200s (C and D) of the process predicted with the S-D model (A and C) and the T-D model (B and D).

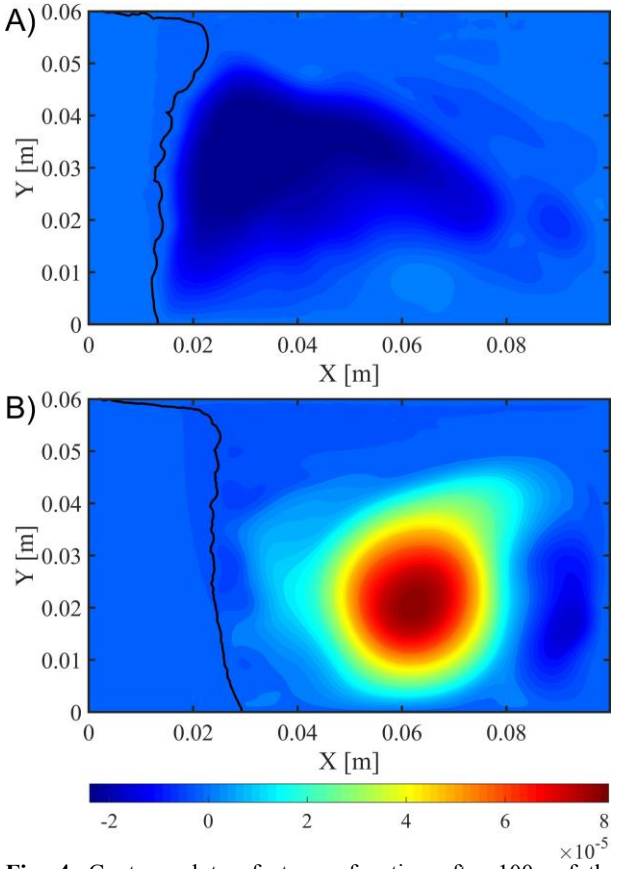

Fig. 4. Contour plots of stream function after 100s of the process predicted with S-D model (A) and T-D model (B).

6 Conclusions

In the proposed paper the mixed model for micro-macroscopic computer simulation of binary alloy solidification is proposed. It involves the mixture approach to modeling the mass, momentum and energy equation and two-domain approach to solute transport. The front tracking procedure is also used to distinguish zones of columnar and equiaxed grains to impose different models of fluid motion and different models of grain growth.

The direct comparison of solid fraction and averaged solute concentration predicted with the proposed model and with the fully equilibrium one shows that actual positions of the boundary between various dendrite morphologies (Fig. 2, 3), as well as fluid flow structure (Fig. 4) differ considerably. Predicted averaged solute concentrations by the two analysed models reveal some similarities, like vertical segregation and the existence of well mixed zone in the slurry region. A disappearance of the segregation channels observed in the proposed model accounting for finite solute diffusion in both phases, at later stage of solidification, requires further study.

References

1. C.Y. Wang, C. Beckermann, Metall. Trans. A **24**, 2787-2802 (1993)
2. D.J. Browne, J.D. Hunt, Numer. Heat Transfer, Part B **45**, 395-419 (2004)

3. J. Banaszek, D.J. Browne, Mater. Trans., JIM **46**, 1378-1387 (2005)
4. M. Seredyński, J. Banaszek, J. Heat Transfer **132**, 102301 (2010)
5. J. Banaszek, M. Seredyński, Int. J. Heat Mass Transfer **55**, 4334–4339 (2012)
6. M. Seredyński, J. Banaszek, Int. J. Numer. Method. H (https://doi.org/10.1108/HFF-11-2018-0712; to be published)
7. O.J. Ilegbusi, M.D. Mat, Mater. Sci. Eng., A **247**, 135-141 (1998)
8. S. Ganesan, D. Poirier, Metall. Trans. B **21**, 173-181 (1990)
9. J. Ni, C. Beckermann, Metall. Trans. B **22**, 349-361 (1991)
10. M.C. Schneider, C. Beckermann, Metall. Mater. Trans. A **26**, 2373-2388 (1995)
11. Y.-J. Jan, T.W.-H. Sheu, Numer. Heat Transfer, Part B **52**, 69-105 (2007)
12. C.M. Rhie, W.L. Chow, AIAA J. **21**, 1525-1532 (1983)